Biochimica et Biophysica Acta 1848 (2015) 422–432

Contents lists available at ScienceDirect

Biochimica et Biophysica Acta

journal homepage: www.elsevier.com/locate/bbamem

Experimental determination and computational interpretation of biophysical properties of lipid bilayers enriched by cholesteryl hemisuccinate

Waldemar Kulig [a,*], Piotr Jurkiewicz [b,*], Agnieszka Olżyńska [b], Joona Tynkkynen [a], Matti Javanainen [a], Moutusi Manna [a], Tomasz Rog [a], Martin Hof [b], Ilpo Vattulainen [a,c], Pavel Jungwirth [a,d]

[a] Department of Physics, Tampere University of Technology, P. O. Box 692, FI-33101 Tampere, Finland
[b] J. Heyrovský Institute of Physical Chemistry, Academy of Sciences of the Czech Republic, v. v. i., Dolejskova 3, 18223 Prague 8, Czech Republic
[c] MEMPHYS-Center for Biomembrane Physics, University of Southern Denmark, Odense, Denmark
[d] Institute of Organic Chemistry Biochemistry, Academy of Sciences of the Czech Republic, Flemingovo nám. 2, 16610 Prague 6, Czech Republic

ARTICLE INFO

Article history:
Received 30 July 2014
Received in revised form 6 October 2014
Accepted 20 October 2014
Available online 25 October 2014

Keywords:
Time-dependent fluorescence shift
Molecular dynamics simulations
Cholesterol-mimicking detergents
Laurdan
DPH
Dynamic light scattering

ABSTRACT

Cholesteryl hemisuccinate (CHS) is one of the cholesterol-mimicking detergents not observed in nature. It is, however, widely used in protein crystallography, in biochemical studies of proteins, and in pharmacology. Here, we performed an extensive experimental and theoretical study on the behavior of CHS in lipid membranes rich in unsaturated phospholipids. We found that the deprotonated form of CHS (that is the predominant form under physiological conditions) does not mimic cholesterol very well. The protonated form of CHS does better in this regard, but also its ability to mimic the physical effects of cholesterol on lipid membranes is limited. Overall, although ordering and condensing effects characteristic to cholesterol are present in systems containing any form of CHS, their strength is appreciably weaker compared to cholesterol. Based on the considerable amount of experimental and atomistic simulation data, we conclude that these differences originate from the fact that the ester group of CHS does not anchor it in an optimal position at the water–membrane interface. The implications of these findings for considerations of protein–cholesterol interactions are briefly discussed.

1. Introduction

Biological membranes are essential parts of living cells. They provide a highly selective permeable barrier for cells, in which the interactions between lipids and proteins allow fundamental processes such as photosynthesis, signal transduction, perspiration, and transport of ions and nonpolar molecules to take place. In essence, biological membranes are comprised of a lipid bilayer that acts as a host to numerous membrane proteins embedded in the bilayer. The specific and usually strong interactions between lipids and proteins play an important role in maintaining the structure and function of membrane proteins; protein crystal structures thus often contain lipids or their fragments co-crystallized together with the protein. In many cases [1–6], cholesterol (CHOL) has been resolved as a part of the protein crystal structure. Such proteins are thereby known as cholesterol-binding and it is assumed that cholesterol has an important effect on their function, such as an ability to promote thermal stability or to induce conformational changes in protein structure. In many cases, however, the cholesterol-type molecules involved in crystal structures are actually not cholesterol but cholesteryl hemisuccinate [7–9]. Cholesteryl hemisuccinate (CHS) is one of the cholesterol-mimicking detergents that is not present in nature, but is widely used in protein crystallography, in biochemical studies of proteins, and in pharmacology. CHS is more soluble in water than cholesterol and, therefore, easier to use in biochemical studies of proteins. It is commercially available and shares an identical structure with CHOL in the nonpolar part of the membrane where many of the key effects of CHOL originate. Therefore, it is understandable that CHS is commonly employed to replace CHOL in studies of the effects of membrane composition on structure and stability of various proteins (especially G-protein coupled receptors) [7,10–14].

CHOL is known to increase the mechanical strength of lipid membranes and decrease membrane permeability to water, small molecules, and ions [15]. Due to these properties CHOL has applications in drug delivery where it is widely employed in the production of liposomes [16]. For this reason, CHS has been tested as a potential component of drug delivery systems. CHS can form pH-sensitive liposomes [17,18] designed to undergo rapid destabilization in an acidic environment [19]. Such a condition occurs after cellular uptake of liposomes in endocytic vesicles. pH-sensitive liposomes have been shown to be more efficient in delivering their contents to the cells than traditional

* Corresponding authors.
E-mail addresses: waldemar.kulig@tut.fi (W. Kulig), piotr.jurkiewicz@jh-inst.cas.cz (P. Jurkiewicz).

http://dx.doi.org/10.1016/j.bbamem.2014.10.032
0005-2736/

ones [20]. CHS may also be used in combination with polymers to coat liposomes to form so-called stealth-pH sensitive liposomes, and it is used in gene delivery where together with other lipids it coats the so-called polyplex-complex of DNA with polymers [21].

For reasons listed above, it is important to know how well CHS can mimic the behavior of CHOL in lipid bilayers. CHOL and ergosterol are the most common sterols in nature, yet various other naturally occurring and synthetic sterols exist, too. The key effects that CHOL has on lipids are the so-called ordering effect (increase of acyl chain order in bilayers with CHOL) and the condensing effect (decrease of surface area per lipid) [22,23]. Numerous studies have shown that even small modifications in CHOL structure modify both effects, typically decreasing their magnitude [24–28]. This also concerns modifications of the polar part of cholesterol. For instance, the change of conformation of the hydroxyl group from beta to alpha [29] or esterification [30] with sulfuric acid has been shown to decrease cholesterol's effects on membrane properties. What is more, even seemingly tiny changes in cholesterol structure, such as a change of an individual double bond to a single one, have been shown to change the function of cholesterol, e.g., replacing cholesterol with desmosterol in raft membranes was reported to impair the function of the insulin receptor [31].

Biophysical studies on the effects of CHS are rather limited. CHS has been shown to act as a membrane stabilizer in the preparation of liposomes [32,33] and it has been found to alter the motion of acyl chains and the fluidity of cell membranes [34,35]. Experimental studies comparing the properties of CHS- and CHOL-containing bilayers have shown that CHS affects their properties less than CHOL [36]. Our recent atomistic molecular dynamics (MD) simulations on the behavior of CHS in saturated lipid bilayers [37] indicated that the protonated version of cholesteryl hemisuccinate (CHS_{prot}) mimics many of the membrane properties of cholesterol quite well, while the deprotonated version (CHS_{deprot}) is less appropriate for this purpose.

Here, we apply time-resolved fluorescence spectroscopy and dynamic light scattering experiments, assisted by atomistic molecular dynamics simulations to study the effects of CHS vs. CHOL on unsaturated lipid bilayers. Our main objective is to clarify how well CHS is able to mimic the physical behavior of cholesterol in membranes rich in unsaturated phospholipids. In this context, it is important to note that in unsaturated lipid membranes under physiological pH, about 98% of cholesteryl hemisuccinate is in its deprotonated state (CHS_{deprot}), since its pKa is about 5.8 [17]. Therefore, given that the experiments reported in this work were carried out at pH equal to 7.4, their results correspond to the deprotonated CHS (CHS_{deprot}). In MD simulations, we yet considered both states (CHS_{prot}, CHS_{deprot}) in order to explore the dependence of CHS behavior on protonation. Building on our previous computational evidence from saturated bilayers [37], we can expect properties of membranes with cholesteryl hemisuccinate (in both protonated and deprotonated forms) to differ from those containing cholesterol. Indeed, the present experiments and simulations demonstrate that, compared to cholesterol, cholesterol hemisuccinate has a smaller condensing effect on the lipid bilayer, making the bilayer less ordered and restricting less the lipid mobility at the glycerol level. This may alter the strength and dynamics of protein–lipid interactions, indicating that cholesteryl hemisuccinate may not be an ideal cholesterol-mimicking detergent for sterol–protein co-crystallization.

2. Materials and methods

2.1. Chemicals and liposome preparation

POPC (1-palmitoyl-2-oleoyl-*sn*-glycero-3-phosphocholine) and CHOL (ovine wool cholesterol) were obtained from Avanti Polar Lipids, Inc. (Alabaster, AL, USA). CHS (cholesteryl hemisuccinate), POPOP (2,2′-(1,4-phenylene)bis[5-phenyl-oxazole]), NaCl, and NaOH were obtained from Sigma-Aldrich (St. Louis, MO, USA). Fluorescent probes: DPH (1,6-diphenyl-1,3,5-hexatriene), and Laurdan (6-lauroyl-2-dimethylaminonaphthalene) were purchased from Invitrogen (Eugene, OR, USA). Hepes (4-(2-hydroxyethyl)-1-piperazineethanesulfonic acid) buffer (Fluka, Buchs, Switzerland) was dissolved in Mili Q water (Milipore, USA). Organic solvents of spectroscopic grade were supplied by Merck (Darmstadt, Germany). All chemicals were used without further purification.

Extruded large unilamellar vesicles (LUVs) were prepared as follows: The appropriate volumes of chloroform solutions of POPC, and either CHS or CHOL, were mixed with methanol solution of a fluorescent probe. Final molar ratio of lipids to probe was 100:1. The organic solvents were evaporated under a stream of nitrogen and then under vacuum overnight. The dried lipid film was suspended in Hepes buffer: 10 mM, pH 7.4 (NaOH), 150 mM NaCl. After 4 min of continuous vortexing the suspension of multilamellar vesicles was extruded through polycarbonate membranes with a nominal pore diameter of 100 nm (Avestin, Ottawa, Canada).

2.2. Dynamic light scattering

The samples were transferred to UV grade poly(methyl methacrylate) cuvettes (Kartell, Noviglio, Italy), and equilibrated at 298 K for 3 min before each measurement. The light scattering setup of Zetasizer Nano ZS (Malvern Instruments Ltd., Worcestershire, UK) consisted of a He–Ne laser (532 nm) and an avalanche photodiode detector (APD). The scattering intensity was collected at the angle of 173°. Intensity-weighted size distributions were obtained using regularized fitting implemented in Zetasizer Software 6.2 (Malvern Instruments Ltd., Worcestershire, UK).

2.3. Fluorescence instrumentation

All fluorescence measurements were performed in 1 cm quartz cuvettes. Temperature was maintained at 310 ± 0.5 K using a water-circulating thermostat. Samples were equilibrated for 10 min before each measurement. Steady-state fluorescence spectra were collected using a Fluorolog-3 spectrofluorimeter (model FL3-11, JobinYvon Inc., Edison, NJ, USA). Fluorescence decays were recorded on a time-correlated single-photon counting (TCSPC) spectrometer: model 5000 U SPC equipped with a NanoLED 11 laser diode (370 nm peak wavelength, 80 ps pulse width, 1 MHz repetition rate) and a cooled Hamamatsu R3809U-50 microchannel plate photomultiplier (IBH, Glasgow, UK). The emission wavelengths were chosen using monochromators. 399 nm cutoff filter was used to eliminate scattered light. The signal level was kept below 2% of the light source repetition rate (1 MHz). Data was collected in 8192 channels (0.014 ns channel width) until the peak value reached 5000 counts. The full width at half maximum (FWHM) of the instrument response function was 85 ps.

2.4. Laurdan fluorescence (GP and TDFS)

Laurdan-labeled LUVs dispersion with 1 mM total lipid concentration was investigated. Steady-state emission spectrum (EX = 373 nm) and two excitation spectra (EM = 440, and 490 nm) were recorded. The excitation spectra were used to calculate excitation generalized polarization spectra (GP_{EX}) [38]:

$$GP_{EX}(\lambda_{EX}) = \frac{I_{440} - I_{490}}{I_{440} + I_{490}} \quad (1)$$

where I_{440} and I_{490} represent fluorescence intensities emitted at 440 nm and 490 nm, respectively (excited at excitation wavelength λ_{EX}).

For time-dependent fluorescence shift method (TDFS), fluorescence emission decays were measured at a series of emission wavelengths (400–540 nm with a 10 nm step). The decays were fitted in DAS6 software (IBH, Glasgow, UK) with multi-exponential function using reconvolution method. The fitted fluorescence decays together with

the steady-state emission spectrum were used to reconstruct time-resolved emission spectra (TRES) according to Ref. [39]. The reconstruction routine was implemented in Matlab R2010b (MathWorks, Natick, MA, USA). The position of TRES maximum, $\nu(t)$, and its full-width at half-maximum, FWHM(t), were inspected. Two main parameters describing polarity and mobility of the probed system were derived from $\nu(t)$. Total emission shift, $\Delta\nu$, reflecting polarity of the probe environment was calculated as:

$$\Delta\nu = \nu(0) - \nu(\infty), \tag{2}$$

where $\nu(0) = \nu_{est}(0) = 23800\ cm^{-1}$ is the position of TRES maximum at $t = 0$ estimated using the method of Fee and Maroncelli [40] and $\nu(\infty)$ stands for the position of the TRES from the fully relaxed state. The dynamics of the polar moieties in the vicinity of the probe was evaluated in terms of the mean integrated relaxation time, τ_r, defined as

$$\tau_r = \int_0^\infty \frac{\nu(t) - \nu(\infty)}{\nu(0) - \nu(\infty)} dt. \tag{3}$$

The percentage of the relaxation process that was faster than the resolution of the instrumentation (~20 ps) was calculated as:

$$\%TDFS_{fast} = \frac{\nu_{est}(0) - \nu_{rec}(0)}{\nu_{est}(0) - \nu(\infty)}, \tag{4}$$

where "rec" subscript indicates a $\nu(0)$ value obtained directly from a TRES reconstruction. This value did not exceed 20% for any of the samples measured. Intrinsic uncertainties for the TDFS parameters were 50 cm^{-1}, and 0.05 ns for $\Delta\nu$, and τ_r, respectively. Further details of TDFS method can be found in Refs. [41,42].

2.5. DPH anisotropy

Steady-state anisotropy (r_{SS}) was measured for LUVs (0.2 mM total lipid concentration) at 357 nm excitation. For each sample, three anisotropy emission scans (420–440 nm) were performed by collecting 4 different fluorescence intensities: I_{HH}, I_{HV}, I_{VV}, and I_{VH}, where in I_{XY}—X and Y stand for the orientation of excitation and emission polarizers, respectively (V—vertical, H—horizontal). r_{SS} was calculated according to the formula:

$$r_{SS} = \frac{I_{VV} - G \cdot I_{VH}}{I_{VV} + 2G \cdot I_{VH}}, \quad G = \frac{I_{HV}}{I_{HH}} \tag{5}$$

All r_{SS} values obtained for the same sample were averaged and a standard uncertainty of the mean was calculated.

Emission intensities for time-resolved anisotropy ($I_{VV}(t)$ and $I_{VH}(t)$) were obtained using reconvolution fitting of the measured decays (EX/EM = 373/466 nm) with the following functions:

$$\begin{aligned} I_{VV}(t) &= G\int_{-\infty}^{t} IRF(t') \frac{1}{3}\left(\alpha_1 e^{-\frac{t-t'}{\tau_1}} + \alpha_2 e^{-\frac{t-t'}{\tau_2}}\right)\left\{1 + 2\left[r_\infty + (r_0 - r_\infty)e^{-\frac{t-t'}{\varphi}}\right]\right\} dt' \\ I_{VH}(t) &= \int_{-\infty}^{t} IRF(t') \frac{1}{3}\left(\alpha_1 e^{-\frac{t-t'}{\tau_1}} + \alpha_2 e^{-\frac{t-t'}{\tau_2}}\right)\left\{1 - \left[r_\infty + (r_0 - r_\infty)e^{-\frac{t-t'}{\varphi}}\right]\right\} dt', \end{aligned} \tag{6}$$

where *IRF* is the instrument response function measured for scattering solution, α_i stands for the amplitude of the i^{th} fluorescence decay component with lifetime τ_i, r_0 is the initial anisotropy, r_∞ is the residual anisotropy and φ stands for the lifetime (rotational correlation time) of the anisotropy decay. G-factor was calculated by applying a tail matching method to the measured standard (ethanol solution of POPOP). The global fitting of the anisotropy decay parameters and the G-factor determination were performed using FluoFit v.4.5 by PicoQuant (Berlin, Germany).

The anisotropy data were evaluated using model introduced by Kinosita, Kawato, and Ikegami [43,44], in which DPH molecule wobbles uniformly in a lipid bilayer within a cone of semiangle θ_c. DPH orientational order parameter was defined [45–47] as

$$S = \sqrt{\frac{r_\infty}{r_0}} = \frac{1}{2}\cos\theta_c(\cos\theta_c + 1). \tag{7}$$

The so-called wobbling diffusion coefficient D_w, defined by Kawato et al. [44], was calculated using the method of Lipari and Szabo [47] from

$$D_W = \frac{1}{\varphi} \cdot \frac{12x^2(x+1)^2 \log\left(\frac{x+1}{2}\right) + 7x^6 - 8x^5 - 22x^4 + 8x^3 + 17x^2 + 4x - 6}{-6(x^5 + x^4 - x^3 - x^2 - 4x + 4)} \tag{8}$$

$$\text{with } x = \cos\theta_c = \frac{\sqrt{8S+1} - 1}{2}$$

2.6. Atomistic MD simulations

All-atom MD simulations were performed for 14 different membrane systems. The first two systems (denoted as DOPC-0 and POPC-0) were bilayers composed of 128 molecules of DOPC or POPC, respectively. The next six systems contained 114 phospholipid molecules (DOPC or POPC) and 14 sterol molecules (CHOL, CHS_{prot}, or CHS_{deprot}), corresponding to a sterol concentration of 10 mol% (for molecular structures, see Fig. 1). These systems are called DOPC_CHOL-10, DOPC_CHS_{prot}-10, DOPC_CHS_{deprot}-10, POPC_CHOL-10, POPC_CHS_{prot}-10, and POPC_CHS_{deprot}-10, in respective order. The last six bilayers were composed of 76 phospholipid molecules (DOPC or POPC) and 52 sterol molecules (CHOL, CHS_{prot}, or CHS_{deprot}), corresponding to a sterol concentration of 40 mol% and denoted as DOPC_CHOL-40, DOPC_CHS_{prot}-40, DOPC_CHS_{deprot}-40, POPC_CHOL-40, POPC_CHS_{prot}-40, and POPC_CHS_{deprot}-40, respectively.

The initial structure of a lipid bilayer was obtained by placing lipid molecules on an 8 × 8 grid resulting in a bilayer comprised of 64 lipids in each leaflet. Initial structures of the sterol-containing bilayers were obtained by randomly exchanging 14 or 52 phospholipid molecules by the sterol molecules. All simulated bilayers were symmetric with regard to lipid composition and adequately hydrated with 6400 water molecules in the simulation box.

Topologies of sterol molecules were built using parameters of existing molecular blocks from the all-atom OPLS (Optimized Parameters for Liquid Simulation) force field [48,49]. Partial charges were taken from the original all-atom OPLS force field. Force field parameters for lipids were taken from Ref. [50]. Additional parameters for a double bond were derived following the same parameterization protocol. Water molecules are described using the TIP3P model [51]. To neutralize bilayers containing charged CHS_{deprot} molecules, sodium ions described by standard OPLS parameters were included in those systems.

The simulation temperature was maintained at 310 K using the Nosé–Hoover thermostat [52,53] with a coupling constant of 0.4 ps. The temperatures of the solute and solvent were controlled independently. Periodic boundary conditions were used in all three directions. The pressure was kept constant with a semi-isotropic scheme, meaning that the pressure in x and y directions (i.e., in the membrane plane) was coupled separately from the pressure in the z (membrane normal) direction. The Parrinello–Rahman barostat [54,55] was used to keep the pressure at 1 atm with a pressure coupling constant of 1 ps and a compressibility of $4.5°10^{-5}\ bar^{-1}$. Long-range electrostatic interactions beyond the non-bonded interaction cutoff of 1.0 nm were treated by the Particle Mesh Ewald scheme (PME) [56] with a Fourier spacing of 0.1 nm and a sixth order interpolation to the Ewald mesh. A long-range dispersion correction to the energy and pressure was added. The LINCS algorithm [57] was used to constrain all covalent bonds, allowing a time step of 2 fs. For water, the SETTLE method [58] was applied.

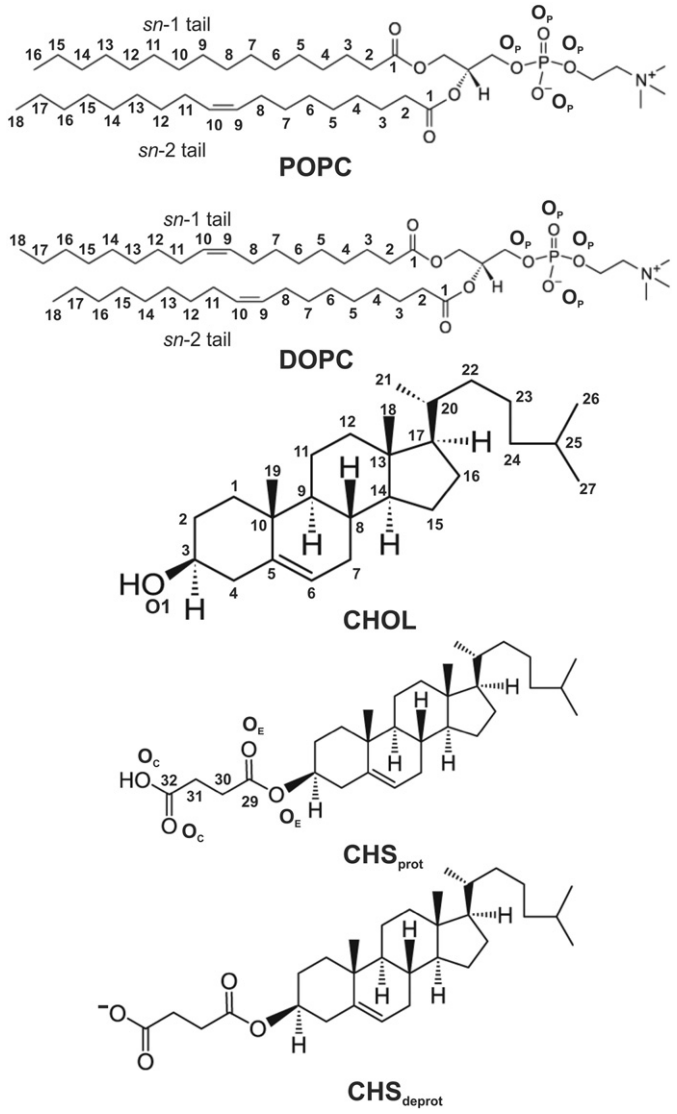

Fig. 1. Chemical structures of 1,2-dioleoyl-*sn*-glycero-3-phosphocholine (DOPC), 1-palmitoyl-2-oleoyl-sn-glycero-3-phosphocholine (POPC), cholesterol (CHOL), and the protonated (CHS_{prot}) and deprotonated (CHS_{deprot}) forms of cholesteryl hemisuccinate (CHS).

The systems were first energy minimized using the steepest descent algorithm followed by an equilibration simulation in the isothermal-isobaric (NpT) ensemble until stable average areas per molecule were obtained. The MD simulations of all bilayer systems were carried out for over 400 ns. The first 200 ns was considered as an equilibration period; thus only the last 200 ns of each trajectory was included in the analyses. All simulations were performed with the GROMACS 4.6.5 software package [59,60]. Altogether the simulations covered a time scale of about 6 ms.

2.7. Analysis of MD data

Several measurable quantities were extracted from the simulation data. The time-dependent area per molecule $A(t)$ was calculated by dividing the total area of the simulation box in the x-y plane by the number of all molecules (phospholipids and sterols) in a single leaflet. Through averaging in equilibrium one then obtains the average area per lipid $\langle A \rangle$. The membrane thickness was calculated as the average inter-leaflet head-to-head (phosphorous atom to phosphorous atom) distance. The average values of the deuterium order parameters [61] ($|S_{CD}|$) were calculated for the acyl chains of lipid molecules using standard GROMACS scripts by averaging over all carbons from the methylene and methyl groups of the lipid molecules' tails (in POPC bilayers over C2–C15 (*sn*-1 tail)) or C2–C17 (*sn*-2 tail) atoms, while in DOPC bilayers over C2–C17 (in both tails)). The tilt angle of the sterol rings was defined as the angle between the C3–C17 vector (see Fig. 1) and the bilayer normal. For evaluation of the average number of contacts between different atomic groups, a cutoff distance of 4 Å (corresponding to the first minimum in the radial distribution function of the cholesterol O1 atom and the choline methyl groups [62]) was used. A contact is considered when the minimum distance between any pair of atoms from the respective groups is equal to or smaller than this cutoff distance. Hydrogen bond is considered to be established when the O – O distance is less than or equal to 3.25 Å and the angle between the O – O vector and the O – H bond is less than or equal to 35° [62].

3. Results and discussion

3.1. In contrast to cholesterol, CHS is fully miscible with POPC

The ability of binary mixtures composed of POPC with either cholesterol or cholesteryl hemisuccinate to form bilayers was measured using dynamic light scattering. Fig. 2 shows the size distributions of extruded samples containing different amounts of either CHS or CHOL mixed with POPC. Here, we remind the reader that

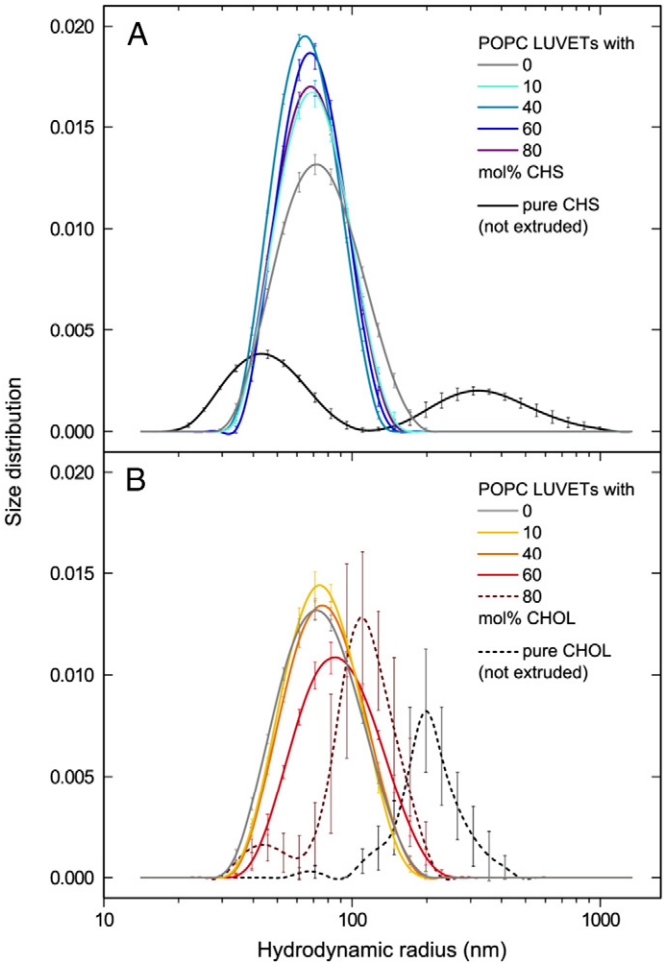

Fig. 2. Size distribution of extruded mixtures of POPC and either CHS (A) or CHOL (B) obtained from DLS measurements. Distributions were normalized so that their areas are equal to 1. The samples with 80 and 100 mol% of cholesterol produced autocorrelation curves that could not be fitted properly; their mean distributions are presented here with their large error bars to indicate their original multimodal distribution.

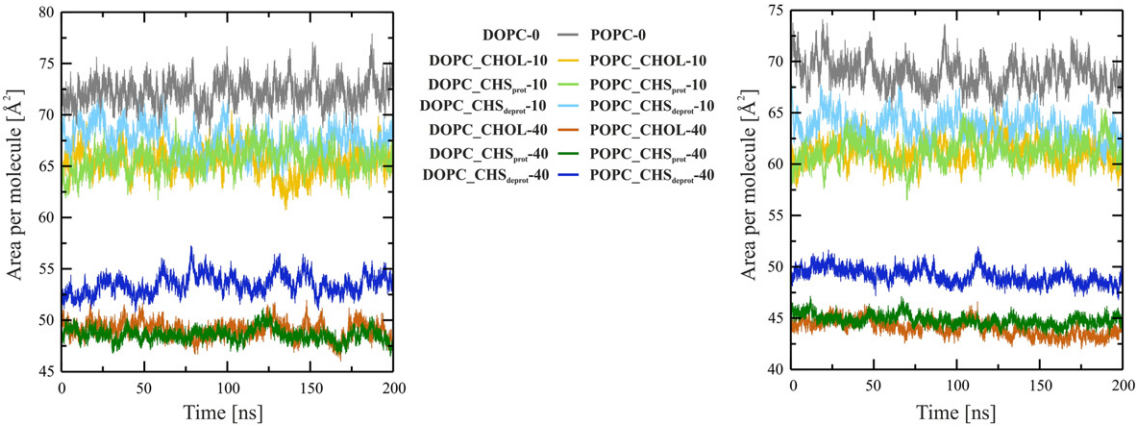

Fig. 3. Area per molecule as a function of simulation time, showing the temporal stability of all bilayer simulations in this study.

the CHS studied in experiments corresponds to the deprotonated state (CHS_{deprot}). Most of the size distributions are unimodal and centered at around 70 nm (hydrodynamic radius), as expected for the large unilamellar vesicles (LUVs) studied. Samples containing 80 and 100 mol% of CHOL were strongly polydisperse and their size distribution thus could not be satisfactorily fitted with any model. Their estimated size distributions with large error bars are presented only to highlight their polydispersity. It is apparent that while CHS is fully miscible with POPC, the situation with cholesterol is different as only up to 60 mol% of CHOL can be added to POPC without disturbing its lamellar phase. The sample consisting of pure CHS was not extruded, though it presents a bimodal size distribution with maxima at 45 and 350 nm. This result is in agreement with the [3H]sucrose encapsulation experiments, which have shown that CHS can form closed membrane vesicles by itself [34].

A further inspection of the unimodal distributions reveals additional differences between CHS and CHOL vesicles. The size of LUVs as well as the width of the distributions increases with increasing CHOL content, but decreases with increasing CHS content. The mean size ± half-width at half-maximum was (73 ± 34) nm, (87 ± 44) nm, and (68 ± 24) nm for pure POPC, 60 mol% CHOL, and 60 mol% CHS, respectively. These results indicate that a CHS/POPC bilayer is more fluid or its spontaneous curvature is larger compared to a pure POPC bilayer. In contrast, a CHOL/POPC bilayer is less fluid or its spontaneous curvature is smaller compared to a pure POPC bilayer.

3.2. CHS condenses lipid bilayers less than cholesterol

The evolution of the area per molecule in time (over the last 200 ns of simulation trajectories) is shown in Fig. 3. The initial evolution of the system (the equilibration stage) is omitted from the presentation in Fig. 3. These plots indicate that the membrane lateral area remains stable in all systems. Averaged values of the area per molecule for all systems considered in this study are shown in Fig. 4 (top row). Calculated values of $\langle A \rangle$ for pure lipid bilayers (72.2 Å^2 and 68.8 Å^2, for pure DOPC and pure POPC bilayers, respectively) are in good agreement with the experimental values measured for fluid bilayers [63,64].

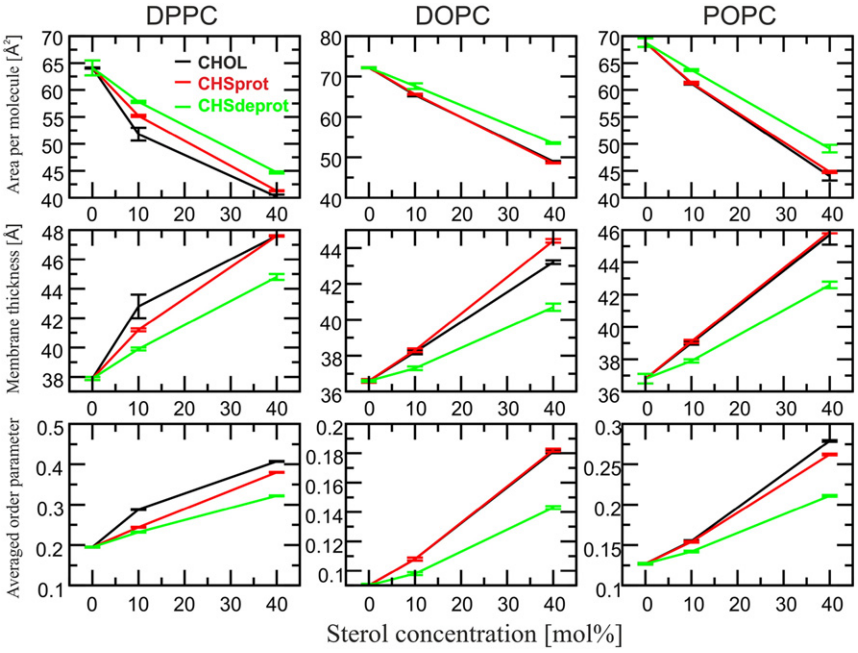

Fig. 4. Average values of area per molecule and bilayer thickness, and average values of deuterium order parameters for the systems studied here through MD simulations. Error bars have been calculated as the standard errors using block averaging. Data for DPPC systems are taken from Ref. [37].

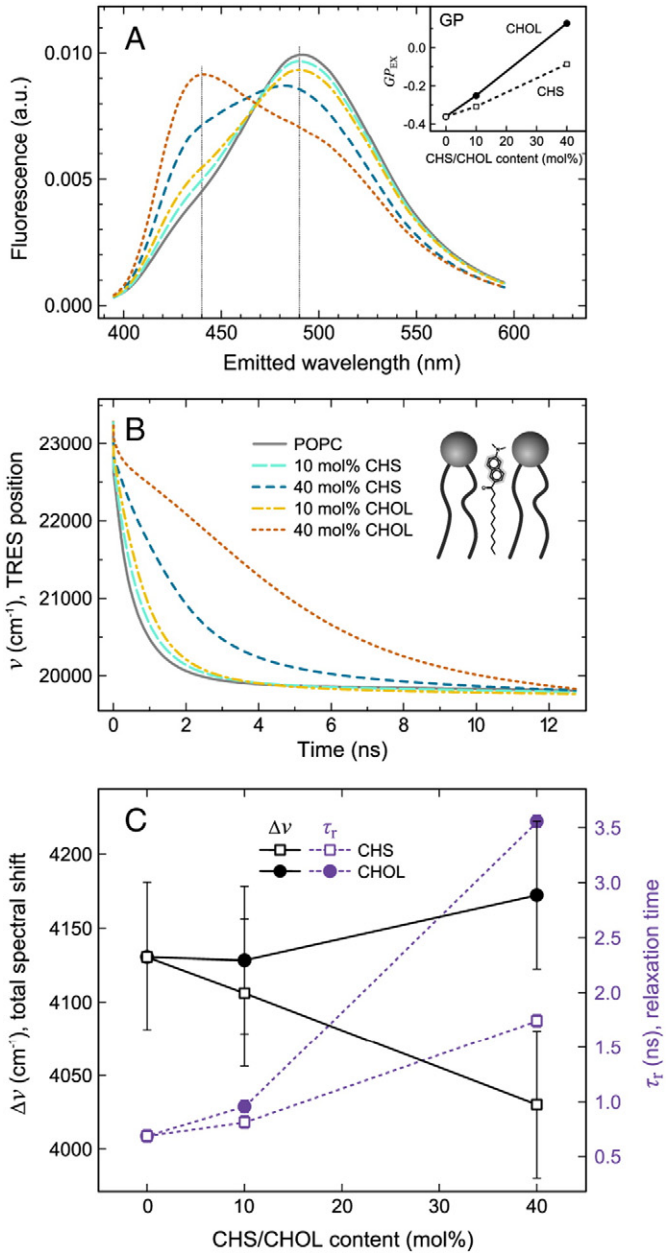

Fig. 5. Fluorescence of Laurdan embedded in large unilamellar vesicles composed of POPC and cholesterol (CHOL) or cholesterol hemisuccinate (CHS), measured at 37 °C. (A) Steady-state emission spectra (mean GP_{EX} (320–380 nm) values are given in the inset). (B) Relaxation curves, i.e. position of the maxima of time-resolved emission spectra (TRES) in time after excitation. (C) Time-dependent fluorescence shift parameters: total spectral shift $\Delta\nu$ and integrated relaxation time τ_r.

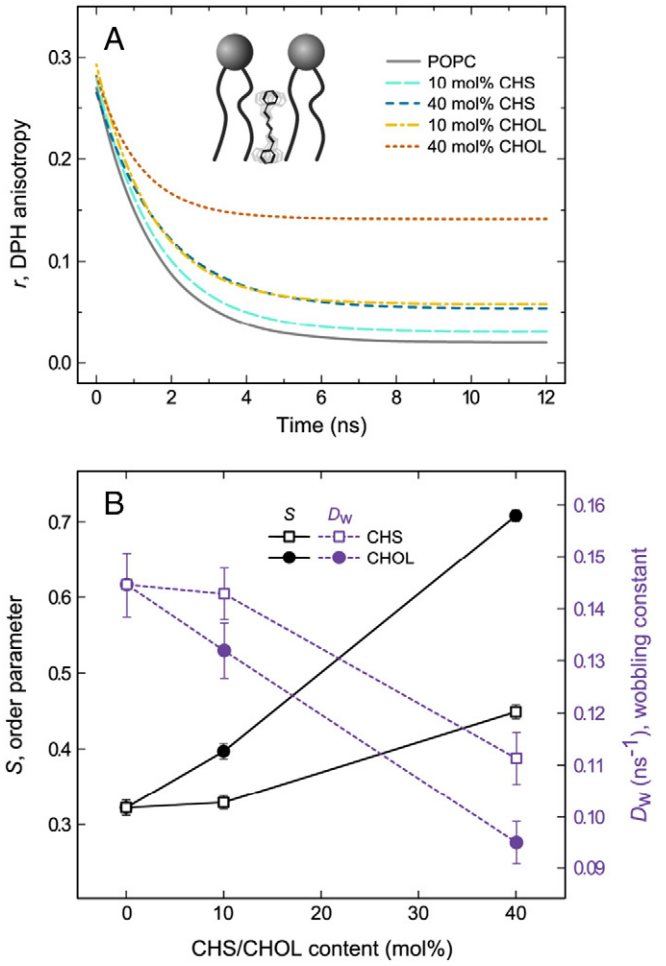

Fig. 6. Time-resolved fluorescence anisotropy of diphenylhexatriene (DPH) embedded in large unilamellar vesicles composed of POPC and cholesterol (CHOL) or cholesterol hemisuccinate (CHS), measured at 37 °C. (A) Anisotropy decays obtained by fitting Eq. (6) to the experimental data. (B) DPH order parameter, and wobbling constant calculated according to the wobbling-in-cone model [43].

The inclusion of all sterol types decreases the average area per molecule (as compared to pure lipid membranes) showing the condensation effect (<*A*> decreases with increasing sterol concentration). In all types of membranes (saturated and unsaturated), the condensation effect of cholesterol is the strongest (resulting in the smallest average area per molecule), followed by CHS_{prot} and CHS_{deprot}. There is one exception to this rule. In the DOPC bilayer containing 40 mol% of sterols, CHS_{prot} condenses the bilayer just as much as cholesterol does.

Sterol addition also substantially affects the thickness of the bilayers (see Fig. 4 (middle row)). It is found to monotonously increase with increasing sterol concentration. Interestingly, the effects of CHOL and CHS_{prot} are virtually of equal magnitude in all membranes, while the effect of the more physiologically relevant CHS_{deprot} is substantially weaker.

3.3. CHS restricts lipid mobility at the glycerol level less than cholesterol does

The results for the average area per molecule obtained from the MD simulations agree with the results of fluorescence measurements performed using a Laurdan probe. Already the steady-state emission spectra of Laurdan show a clear difference between the measured samples (Fig. 5A). A simple quantification of the solvatochromic shift observed for this probe—generalized polarization (GP)—gives different trends for increasing content of CHOL and CHS (inset in Fig. 5A). Those increases in GP values can be interpreted as stiffening or dehydration of the lipid carbonyls that are probed by Laurdan. The effects are considerably stronger for cholesterol than for its succinated form. To distinguish between local lipid mobility and hydration, time-resolved fluorescence data is required. Analysis of the position of time-dependent emission spectra presented in Fig. 5B gives two separate parameters—total emission shift ($\Delta\nu$) for hydration/polarity and integrated relaxation time (τ_r) for local lipid mobility (see Eqs. (2) and (3)). It has been shown that the changes in mobility of hydrated carbonyls often correspond to lateral compression of the lipid bilayer, i.e., τ_r is usually inversely proportional to <*A*> [42]. The values of integrated

Table 1
Average deuterium order parameters and the sterol rings' average tilt angles for the bilayers studied here.

System	Average deuterium order parameters[a]	Average sterol rings tilt angle [°][b]
DOPC-0	0.090	–
DOPC_CHOL-10	0.108	25.9
DOPC_CHS_{prot}-10	0.108	38.1
DOPC_CHS_{deprot}-10	0.098	37.2
DOPC_CHOL-40	0.181	17.8
DOPC_CHS_{prot}-40	0.182	21.5
DOPC_CHS_{deprot}-40	0.143	30.8
POPC-0	0.127	–
POPC_CHOL-10	0.155	25.5
POPC-CHS_{prot}-10	0.154	33.0
POPC_CHS_{deprot}-10	0.142	36.2
POPC_CHOL-40	0.279	14.1
POPC_CHS_{prot}-40	0.262	19.8
POPC_CHS_{deprot}-40	0.211	28.1

[a] Standard error is smaller than 0.001.
[b] Standard error is smaller than 0.02°.

relaxation times τ_r shown in Fig. 5C indicate that the mobility of lipid carbonyls is restricted by both sterols. At 10 mol%, cholesterol slows down the mobility only slightly more than CHS, but at 40 mol% the difference is clearly visible.

The results presented herein for Laurdan are in qualitative agreement with the steady-state results measured for two Laurdan analogs —Prodan and Patman—published by Massey [36], who interpreted the increased GP values as bilayer dehydration. Our time-resolved data show that the increased GP of Laurdan predominantly results from the hindered mobility of the hydrated lipid carbonyls. This is likely to be also the case for Prodan and Patman. We discuss the differences in bilayer polarity/hydration separately below.

3.4. The effect of CHS in affecting acyl chain order and dynamics is inferior compared to cholesterol

CHOL is known to order the acyl chain region of fluid lipid membranes. Here, we compare its ordering effect with that of CHS using DPH anisotropy measurements and MD simulations.

DPH is a rigid hydrophobic rod-like fluorescent probe aligned along the lipid acyl chains in lipid bilayers [65–67], as schematically depicted in Fig. 6. Measurements of DPH anisotropy allow estimation of acyl chain order and mobility [68], though it also has limitations that render its use being most applicable in predicting trends [66]. DPH orientational order parameter S (Eq. (7)) was postulated to be in good agreement with ^{2}D NMR order parameter measured for deuterium atoms located on the 9th or 10th carbon atoms down the lipid acyl chain [45,46]. The time-resolved anisotropy decays, order parameters, and wobbling diffusion coefficients of DPH in the studied bilayers are presented in Fig. 6. The anisotropy decays obtained from the fitting of Eq. (6) to the experimental data are noticeably altered by the presence of both CHOL and CHS (see Fig. 6A). It is evident that the effect of CHS is weaker than that of CHOL. This was also observed in the measured steady-state anisotropy, which provided values of 0.082 ± 0.002, 0.098 ± 0.002, 0.185 ± 0.005, 0.085 ± 0.002, and 0.129 ± 0.004, for POPC, 10 and 40 mol% cholesterol, and 10 and 40 mol% CHS, respectively.

In contrast to the steady-state anisotropy, the time-resolved measurements allow a more accurate characterization of the acyl chain region by distinguishing between structural and dynamic effects. In our case the DPH order parameter (S) and the wobbling diffusion coefficient (D_W) shown in Fig. 6B give a similar picture: while both sterols increase the order and decrease the wobbling constant, CHOL again affects these parameters more than CHS.

Since the DPH order parameter is usually a good approximation of the lipid acyl chain order [45,46,66], we can compare the ordering of CHOL and CHS observed in the experiment with the deuterium order parameter calculated from MD simulations (see Fig. 4). The deuterium order parameter data clearly show that all sterols order the bilayer. CHOL orders the membranes the most, followed by CHS_{prot} and CHS_{deprot}. This picture is independent on the type of the bilayer (saturated [37] or unsaturated). At a higher sterol concentration, differences between sterols are even more enhanced. This fully corroborates with the measured DPH order.

The DPH wobbling diffusion coefficient describes the dynamics of the acyl chain region (Fig. 6B). The value of this parameter is determined by the frequency of collisions between DPH and the neighboring lipids and by the mean free rotational angle between successive collisions [44]. Our results show that CHOL slows down the dynamics of the acyl chain region in a much more efficient manner than to CHS.

The above described time-resolved and steady-state DPH anisotropy results are in close agreement with the steady-state anisotropy measured by Massey [36]. There is reason to bear in mind, though, as it was discussed before, that the experimental results for CHS obtained at pH 7.4 should be compared with CHS_{deprot} rather than with CHS_{prot}.

3.5. Location and orientation of sterols inside the bilayer

Table 1 shows simulation results for the average tilt angle of the sterol ring (for definition see *Analysis of MD data section*). It has been shown previously that the sterol tilt is an appropriate indicator of sterols' ability to order their local surroundings [69], thus comparing the tilt of CHOL and CHS provides one with important insight into their possibly different ordering capabilities. Also, it is important to stress that the average tilt angles change with sterol concentration. In bilayers with a high sterol concentration, sterol rings prefer being almost parallel to the normal of the bilayer, while in bilayers with a smaller sterol concentration they tend to be more tilted. Sterol concentration

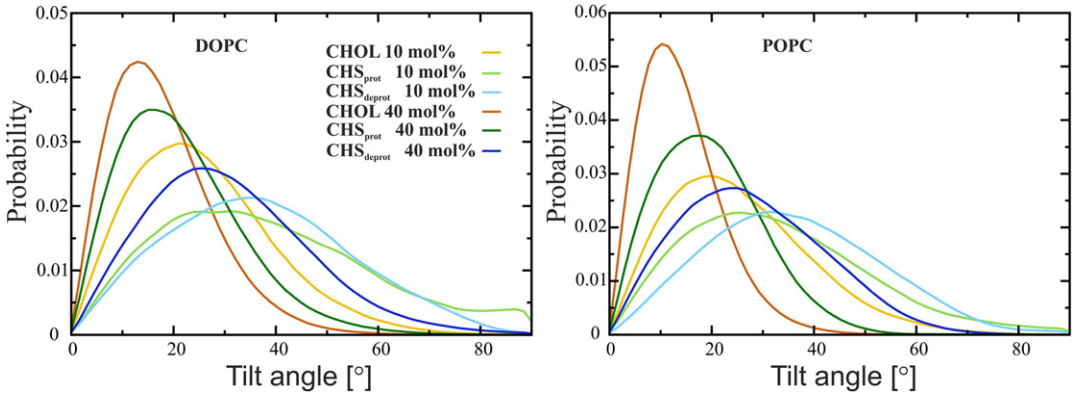

Fig. 7. Distributions of the tilt angle of the sterol ring determined through atomistic MD simulations. See details in the *Analysis of MD data* subsection.

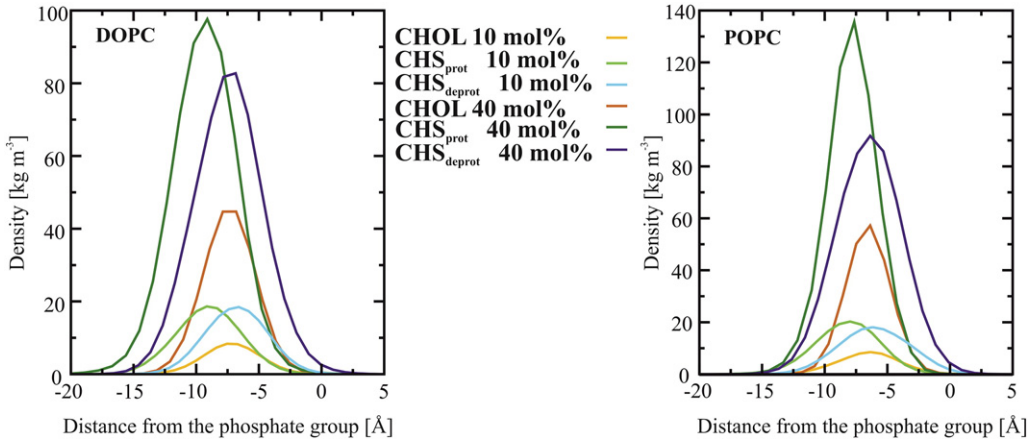

Fig. 8. Partial mass density profiles of a hydroxyl (in CHOL) or ester (in CHS_{prot} and CHS_{deprot}) group along the normal of the bilayer, computed from MD simulations. Profiles were shifted such that the distributions of the phosphate groups in phosphatidylcholine headgroups overlap. Distance of zero corresponds to the position of the phosphate groups.

affects also the widths of the tilt angle distributions shown in Fig. 7, which become narrower with increasing sterol concentration. This agrees with the changes in the average area per molecule (see Fig. 4); in a more tightly packed bilayer (lower area per molecule) sterols cannot tilt as much as in the less crowded ones (higher area per molecule).

Average sterol rings' tilt angles also change with the type of sterol, being the smallest for CHOL, followed by CHS_{prot} and CHS_{deprot}. This may be connected with the flexibility of the sterol molecule. In case of CHOL the functional group pointing out to the membrane–water interface is the hydroxyl group that has less degrees of freedom (and therefore CHOL is less flexible) than the hemisuccinate group of CHS_{prot} and CHS_{deprot} (allowing them to tilt more easily).

To elucidate the location of the sterols inside the phospholipid bilayers, partial mass density profiles were calculated. Fig. 8 shows mass density profiles of the hydroxyl (in CHOL) or ester group (in CHS_{prot} and CHS_{deprot}) of the sterols. Mass profiles of different systems were shifted such that the distributions of the phosphate groups overlap, which allows direct comparison of the depth of the penetration of the bilayer by the sterols' hydrophilic groups. Fig. 8 shows that the ester group of CHS_{prot} is located much deeper than the hydroxyl and ester groups of CHOL and CHS_{deprot}, respectively. The partial mass density profiles of the sterols' rings (C1–C17, see Fig. 1) shown in Fig. 9 seem to corroborate this observation, suggesting that the protonated form of cholesteryl hemisuccinate (CHS_{prot}) penetrates the bilayer much deeper than cholesterol or CHS_{deprot}, and that the bilayer penetration of the last two compounds is almost the same. This behavior is altered by neither the type of the bilayer (similar pattern was also noticed previously in the saturated phospholipid bilayers [37]) nor the sterol concentration.

3.6. Sterols affect the hydration of the carbonyl region of lipids

To elucidate the effect of the sterols on the water–membrane interface, numbers of contacts between all molecules in this region were calculated based on the simulation data. Results of this analysis are listed in Table 2. The number of sterol–lipid interactions seems to be almost the same in all systems taken into consideration in this study. In all cases the addition of a sterol decreases the number of lipid–water interactions (as compared to the pure phospholipid systems). This effect depends on both the concentration of sterol and the sterol type. CHS_{prot} decreases the number of lipid–water interactions the most, followed by CHS_{deprot} and CHOL. This corresponds nicely with the number of water–carbonyl interactions (following the same trend) showing that CHS_{prot} dehydrates the carbonyl region of lipids more effectively than CHS_{deprot} or CHOL.

In TDFS experiments the total spectral shift, $\Delta\nu$, is often directly related to the local polarity and hydration in a membrane [42]. In the present study a precise determination of this parameter was difficult in the case of higher sterol contents. Primarily for 40 mol% of CHOL, but also to some extent for 40 mol% of CHS, the dipolar relaxation was very slow. As a result the TRES position (Fig. 5B) did not converge to a constant value within the fluorescence lifetime of Laurdan. This

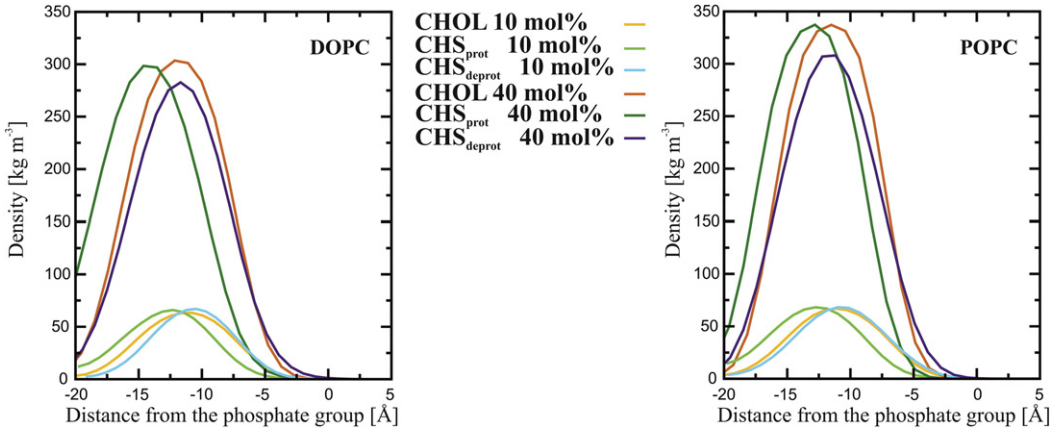

Fig. 9. Partial mass density profiles of the sterol ring's (C1–C17) group along the normal of the bilayer, determined from simulations. Profiles were shifted such the distributions of the phosphate groups in phosphatidylcholine headgroups overlap. Distance of zero corresponds to the position of the phosphate groups.

Table 2
Average number of contacts at the water–membrane interface. Lipid–water and water–carbonyl contacts were normalized to the corresponding values in pure lipid bilayers, while sterol–lipid and sterol–water contacts were normalized to the corresponding values in the systems containing 10 mol% or 40 mol% of cholesterol. Errors are smaller than 1%.

System	Sterol–lipid	Sterol–water	Lipid–water	Water–carbonyl
DOPC-0	–	–	1.00	*sn*-1 1.00
				sn-2 1.00
DOPC_CHOL-10	1.00	1.00	0.89	*sn*-1 0.89
				sn-2 0.90
DOPC_CHS_{prot}-10	1.18	1.17	0.87	*sn*-1 0.88
				sn-2 0.87
DOPC_CHS_{deprot}-10	1.08	2.48	0.89	*sn*-1 0.89
				sn-2 0.88
DOPC_CHOL-40	1.00	1.00	0.59	*sn*-1 0.60
				sn-2 0.61
DOPC_CHS_{prot}-40	1.15	0.92	0.55	*sn*-1 0.54
				sn-2 0.54
DOPC_CHS_{deprot}-40	1.10	2.04	0.58	*sn*-1 0.59
				sn-2 0.55
POPC-0	–	–	1.00	*sn*-1 1.00
				sn-2 1.00
POPC_CHOL-10	1.00	1.00	0.88	*sn*-1 0.86
				sn-2 0.88
POPC_CHS_{prot}-10	1.16	1.16	0.87	*sn*-1 0.85
				sn-2 0.87
POPC_CHS_{deprot}-10	1.10	2.61	0.88	*sn*-1 0.88
				sn-2 0.88
POPC_CHOL-40	1.00	1.00	0.58	*sn*-1 0.57
				sn-2 0.61
POPC_CHS_{prot}-40	1.20	1.15	0.53	*sn*-1 0.49
				sn-2 0.52
POPC_CHS_{deprot}-40	1.07	2.24	0.57	*sn*-1 0.56
				sn-2 0.56

hampered accurate determination of $\nu(\infty)$, which was estimated by extrapolating $\nu(t)$. Therefore the values of $\Delta\nu$ presented herein for systems with 40 mol% sterols should be regarded as suggestive estimates. Addition of 10 mol% of either CHOL or CHS into pure phospholipid bilayers does not change the hydration of the carbonyl region probed by Laurdan (Fig. 5C). The observed slight decrease in $\Delta\nu$ is within the error bars. At 40 mol% CHS already significantly dehydrates the probed region. Surprisingly, $\Delta\nu$ measured for 40 mol% of CHOL is even slightly higher than for the pure POPC bilayer, which is not supported by the MD results. This discrepancy might result from phase separation present in experiments [70] and not observed in MD simulations due to a finite system size considered.

Cholesterol is known to form hydrogen bonds (H-bonds) with carbonyl and phosphate groups of PC molecules. On average in our simulations we observed 0.21–0.29 H-bonds formed between the hydroxyl group of CHOL and phospholipids. CHS_{prot} is also capable to form H-bonds via its protonated carboxyl group and we observe 0.61–0.72 H-bonds formed for CHS_{prot}. The second important interaction between CHOL and phospholipids concerns charge pairs between the negatively charged CHOL oxygen and the positively charged methyl groups of choline. These interactions are sometimes considered as weak hydrogen bonds. For cholesterol's O1 oxygen we observe 1.5–1.65 charge pairs per molecule, while for the O1 oxygen of CHS_{prot} this number is less than 0.1, and for CHS_{deprot} it was found to be 0.14. The carbonyl oxygen O2 is also participating in charge pairs in CHS_{prot}, and the number of charge pairs it forms with phospholipids is less than 0.26. The corresponding value for CHS_{deprot} is 1.1. These differences in the frequency of charge pairs between CHS_{deprot} and CHS_{prot} can be explained by differences in vertical locations of the sterols: CHS_{prot} positions itself much deeper into the lipid bilayer and, therefore, its interactions with choline are less likely. While we compare the mass distribution of O1 of the simulated sterols along the bilayer normal, we see that this distribution is narrower for CHOL compared to both forms of CHS. The corresponding full widths at half maximum are (5.2 ± 0.1)Å, (6.1 ± 0.2)Å, (6.0 ± 0.2)Å, (5.0 ± 0.1)Å, (6.0 ± 0.2)Å, (6.3 ± 0.2)Å, (5.5 ± 0.1)Å, (6.1 ± 0.2)Å, (6.9 ± 0.2)Å, (4.2 ± 0.1)Å, (7.0 ± 0.2)Å, and (6.3 ± 0.1)Å for DOPC_CHOL_10, DOPC_CHS_{prot}_10, DOPC_CHS_{deprot}_10, DOPC_CHOL_40, DOPC_CHS_{prot}_40, DOPC_CHS_{deprot}_40, POPC_CHOL_10, POPC_CHS_{prot}_10, POPC_CHS_{deprot}_10, POPC_CHOL_40, POPC_CHS_{prot}_40, and POPC_CHS_{deprot}_40, respectively. This results from the lower ability of CHS to form charge pairs with choline groups and the lack of ability of forming H-bonds which seems to anchor cholesterol in its optimal position. These dissimilarities also explain the difference in the mobility of the carbonyl region as discussed above—narrower distribution indicates that the protrusive motion of cholesterol is more restricted than that of both forms of CHS. The carboxylic group of CHS also interacts with choline groups. However, as it is located at the flexible chain it does not contribute to anchoring the molecule in a specific position. The carboxylic group of CHS_{prot} forms 3.0 charge pairs while that of CHS_{deprot} forms 4.5 such pairs.

4. Summary and conclusions

Cholesteryl hemisuccinate, a convenient synthetic surrogate for cholesterol in protein crystallization, should be used with care. We have shown that the substitution of cholesteryl hemisuccinate for cholesterol in model lipid membranes changes the physical properties of a membrane significantly. Full miscibility of CHS with POPC can be advantageous for biochemical studies, but our DLS measurements show that the resulting lipid membrane is easier to deform, while fluorescence measurements indicate acyl chain disordering and increased lipid mobility. All-atom MD simulations confirm decreased lipid packing and provide a molecular view on the CHS-containing bilayers. The deprotonated form of CHS (CHS_{deprot}), while located at the same depth in a lipid bilayer (compared to cholesterol), is more tilted than cholesterol, which is in line with the elevated area per lipid of CHS_{deprot}-containing membranes. This result is quite striking, since it is the deprotonated version CHS_{deprot} that is more abundant under physiological pH compared to the protonated CHS_{prot}. Yet, when we consider all the present data together, CHS_{prot} mimics cholesterol behavior better compared to CHS_{deprot}.

The changes due to CHS described herein for unsaturated lipid bilayers (POPC and DOPC) are in qualitative agreement with the results of MD simulations of CHS-containing saturated lipid bilayers that we published recently [37]. Yet the present data show that in lipid bilayers comprised mainly of unsaturated lipids the differences of CHS compared to CHOL are a bit stronger compared to those in a saturated lipid environment. Further, the present study also unravels the role of CHS protonation through a comparison of protonated (CHS_{prot}) versus deprotonated (CHS_{deprot}) forms of CHS. The latter form should prevail under physiological pH. Our results demonstrate that the discrepancy between the properties of cholesterol and CHS is much stronger for the deprotonated form of CHS.

The function of many transmembrane proteins can be modulated by their interactions with neighboring lipids [71]. Thus, the differences between cholesterol and CHS in their ordering and condensing effects we have observed in model lipid membranes could easily affect protein–lipid interaction in biological membranes. This is why the use of this cholesterol-mimicking detergent for sterol–protein co-crystallization might lead to unreliable protein structures. We predict that this difficulty may become even more pronounced for the membrane proteins that are known to directly interact with cholesterol, either specifically [72] or non-specifically [73]. We plan to address this issue in our future work.

Acknowledgments

We thank the Academy of Finland for financial support (the Finland Distinguished Professor (FiDiPro, grant number 263410) program (WK,

PJ), and the Centre of Excellence (MJ, JT, MM, TR, IV) funding (grant number 272130)). PJ, MH, AO, and PJ thank the Czech Science Foundation (grant P208/12/G016). MH and PJ acknowledge the Academy of Sciences for the Praemium Academie awards. IV thanks the European Research Council (Advanced Grant CROWDED-PRO-LIPIDS). MJ thanks the Finnish Doctoral Programme in Computational Sciences (FICS). CSC—IT Center for Science (Espoo, Finland) is acknowledged for excellent computational resources (project number tty3995).

References

[1] W. Liu, E. Chun, A.A. Thompson, P. Chubukov, F. Xu, V. Katritch, G.W. Han, C.B. Roth, L.H. Heitman, A.P. Ijzerman, V. Cherezov, R.C. Stevens, Structural basis for allosteric regulation of GPCRs by sodium ions, Science 337 (2012) 232–236.
[2] V. Cherezov, D.M. Rosenbaum, M.A. Hanson, S.G.F. Rasmussen, F.S. Thian, T.S. Kobilka, H.J. Choi, P. Kuhn, W.I. Weis, B.K. Kobilka, R.C. Stevens, High-resolution crystal structure of an engineered human beta(2)-adrenergic G protein-coupled receptor, Science 318 (2007) 1258–1265.
[3] J.P. Morth, B.P. Pedersen, M.S. Toustrup-Jensen, T.L.M. Sorensen, J. Petersen, J.P. Andersen, B. Vilsen, P. Nissen, Crystal structure of the sodium–potassium pump, Nature 450 (2007) U1043–U1046.
[4] M. Laursen, L. Yatime, P. Nissen, N.U. Fedosova, Crystal structure of the high-affinity Na+, K+-ATPase-ouabain complex with Mg2+ bound in the cation binding site, Proc. Natl. Acad. Sci. U. S. A. 110 (2013) 10958–10963.
[5] H.J. Kwon, L. Abi-Mosleh, M.L. Wang, J. Deisenhofer, J.L. Goldstein, M.S. Brown, R.E. Infante, Structure of N-terminal domain of NPC1 reveals distinct subdomains for binding and transfer of cholesterol, Cell 137 (2009) 1213–1224.
[6] M.B. Lascombe, M. Ponchet, P. Venard, M.L. Milat, J.P. Blein, T. Prange, The 1.45 angstrom resolution structure of the cryptogein-cholesterol complex: a close-up view of a sterol carrier protein (SCP) active site, Acta Crystallogr. D Biol. Crystallogr. 58 (2002) 1442–1447.
[7] M. Zocher, C. Zhang, S.G.F. Rasmussen, B.K. Kobilka, D.J. Müller, Cholesterol increases kinetic, energetic, and mechanical stability of the human beta(2)-adrenergic receptor, Proc. Natl. Acad. Sci. U. S. A. 109 (2012) E3463–E3472.
[8] J.A. Christopher, J. Brown, A.S. Dore, J.C. Errey, M. Koglin, F.H. Marshall, D.G. Myszka, R.L. Rich, C.G. Tate, B. Tehan, T. Warne, M. Congreve, Biophysical fragment screening of the beta(1)-adrenergic receptor: identification of high affinity arylpiperazine leads using structure-based drug design, J. Med. Chem. 56 (2013) 3446–3455.
[9] T. Warne, R. Moukhametzianov, J.G. Baker, R. Nehme, P.C. Edwards, A.G.W. Leslie, G.F.X. Schertler, C.G. Tate, The structural basis for agonist and partial agonist action on a beta(1)-adrenergic receptor, Nature 469 (2011) 241–244.
[10] M.A. O'Malley, M.E. Helgeson, N.J. Wagner, A.S. Robinson, The morphology and composition of cholesterol-rich micellar nanostructures determine transmembrane protein (GPCR) activity, Biophys. J. 100 (2011) L11–L13.
[11] M.A. O'Malley, M.E. Helgeson, N.J. Wagner, A.S. Robinson, Toward rational design of protein detergent complexes: determinants of mixed micelles that are critical for the in vitro stabilization of a G-protein coupled receptor, Biophys. J. 101 (2011) 1938–1948.
[12] A.A. Thompson, J.J. Liu, E. Chun, D. Wacker, H.X. Wu, V. Cherezov, R.C. Stevens, GPCR stabilization using the bicelle-like architecture of mixed sterol-detergent micelles, Methods 55 (2011) 310–317.
[13] K. Vukoti, T. Kimura, L. Macke, K. Gawrisch, A. Yeliseev, Stabilization of functional recombinant cannabinoid receptor CB2 in detergent micelles and lipid bilayers, Plos One 7 (2012) 19.
[14] J. Oates, B. Faust, H. Attrill, P. Harding, M. Orwick, A. Watts, The role of cholesterol on the activity and stability of neurotensin receptor 1, Biochim. Biophys. Acta Biomembr. 1818 (2012) 2228–2233.
[15] S. Shinozawa, Y. Araki, K. Utsumi, T. Oda, Stabilizing effects of cholesterol on changes in membrane-permeability and potential induced in red blood-cells by lysolecithin, Physiol. Chem. Phys. 11 (1979) 161–167.
[16] A. Gabizon, R. Catane, B. Uziely, B. Kaufman, T. Safra, R. Cohen, F. Martin, A. Huang, Y. Barenholz, Prolonged circulation time and enhanced accumulation in malignant exudates of doxorubicin encapsulated in polyethylene-glycol coated liposomes, Cancer Res. 54 (1994) 987–992.
[17] I.M. Hafez, P.R. Cullis, Cholesteryl hemisuccinate exhibits pH sensitive polymorphic phase behavior, Biochim. Biophys. Acta Biomembr. 1463 (2000) 107–114.
[18] S. Simoes, J.N. Moreira, C. Fonseca, N. Duzgunes, M.C.P. de Lima, On the formulation of pH-sensitive long circulation times, Adv. Drug Deliv. Rev. 56 (2004) 947–965.
[19] R.M. Straubinger, pH-sensitive liposomes for delivery of macromolecules into cytoplasm of cultured-cells, Methods Enzymol. 221 (1993) 361–376.
[20] N. Skalko-Basnet, M. Tohda, H. Watanabe, Uptake of liposomally entrapped fluorescent antisense oligonucleotides in NG108-15 cells: conventional versus pH-sensitive, Biol. Pharm. Bull. 25 (2002) 1583–1587.
[21] J. Lehtinen, Z. Hyvonen, A. Subrizi, H. Bunjes, A. Urtti, Glycosaminoglycan-resistant and pH-sensitive lipid-coated DNA complexes produced by detergent removal method, J. Control. Release 131 (2008) 145–149.
[22] D. Marsh, I.C.P. Smith, An interacting spin label study of the fluidizing and condensing effects of cholesterol on lecithin bilayers, Biochim. Biophys. Acta 298 (1973) 133–144.
[23] P.L. Yeagle, Cholesterol and the cell-membrane, Biochim. Biophys. Acta 822 (1985) 267–287.
[24] H.A. Scheidt, T. Meyer, J. Nikolaus, D.J. Baek, I. Haralampiev, L. Thomas, R. Bittman, P. Mueller, A. Herrmann, D. Huster, Cholesterol's aliphatic side chain modulates membrane properties, Angew. Chem. Int. Ed. 52 (2013) 12848–12851.
[25] S. Poyry, T. Rog, M. Karttunen, I. Vattulainen, Significance of cholesterol methyl groups, J. Phys. Chem. B 112 (2008) 2922–2929.
[26] T. Rog, M. Pasenkiewicz-Gierula, I. Vattulainen, M. Karttunen, What happens if cholesterol is made smoother: importance of methyl substituents in cholesterol ring structure on phosphatidylcholine–sterol interaction, Biophys. J. 92 (2007) 3346–3357.
[27] T. Rog, M. Pasenkiewicz-Gierula, I. Vattulainen, M. Karttunen, Ordering effects of cholesterol and its analogues, Biochim. Biophys. Acta Biomembr. 1788 (2009) 97–121.
[28] M. Pourmousa, T. Róg, R. Mikkeli, I. Vattulainen, L.M. Solanko, D. Wüstner, N.H. List, J. Kongsted, M. Karttunen, Dehydroergosterol as an analogue for cholesterol: why it mimics cholesterol so well—or does it? J. Phys. Chem. B 118 (2014) 7345–7357.
[29] T. Rog, M. Pasenkiewicz-Gierula, Effects of epicholesterol on the phosphatidylcholine bilayer: a molecular simulation study, Biophys. J. 84 (2003) 1818–1826.
[30] A.M. Smondyrev, M.L. Berkowitz, Molecular dynamics simulation of dipalmitoylphosphatidylcholine membrane with cholesterol sulfate, Biophys. J. 78 (2000) 1672–1680.
[31] S. Vainio, M. Jansen, M. Koivusalo, T. Rog, M. Karttunen, I. Vattulainen, E. Ikonen, Significance of sterol structural specificity—desmosterol cannot replace cholesterol in lipid rafts, J. Biol. Chem. 281 (2006) 348–355.
[32] G.J. Zhang, H.W. Liu, L. Yang, Y.G. Zhong, Y.Z. Zheng, Influence of membrane physical state on the lysosomal proton permeability, J. Membr. Biol. 175 (2000) 53–62.
[33] W.X. Ding, X.R. Qi, P. Li, Y. Maitani, T. Nagai, Cholesteryl hemisuccinate as a membrane stabilizer in dipalmitoylphosphatidylcholine liposomes containing saikosaponin-d, Int. J. Pharm. 300 (2005) 38–47.
[34] M.Z. Lai, N. Duzgunes, F.C. Szoka, Effects of replacement of the hydroxyl group of cholesterol and tocopherol on the thermotropic behavior of phospholipid-membranes, Biochemistry 24 (1985) 1646–1653.
[35] D. Dumas, S. Muller, F. Gouin, F. Baros, M.L. Viriot, J.F. Stoltz, Membrane fluidity and oxygen diffusion in cholesterol-enriched erythrocyte membrane, Arch. Biochem. Biophys. 341 (1997) 34–39.
[36] J.B. Massey, Effect of cholesteryl hemisuccinate on the interfacial properties of phosphatidylcholine bilayers, Biochim. Biophys. Acta Biomembr. 1415 (1998) 193–204.
[37] W. Kulig, J. Tynkkynen, M. Javanainen, M. Manna, T. Rog, I. Vattulainen, P. Jungwirth, How well does cholesteryl hemisuccinate mimic cholesterol in saturated phospholipid bilayers? J. Mol. Model. 20 (2014).
[38] T. Parasassi, G. De Stasio, A. Dubaldo, E. Gratton, Phase fluctuations in phospholipid-membranes revealed by Laurdan fluorescence, Biophys. J. 57 (1990) 1179–1186.
[39] M.L. Horng, J.A. Gardecki, A. Papazyan, M. Maroncelli, Subpicosecond measurements of polar solvation dynamics—coumarin-153 revisited, J. Phys. Chem. 99 (1995) 17311–17337.
[40] R.S. Fee, M. Maroncelli, Estimating the time-zero spectrum in time-resolved emission measurements of solvation dynamics, Chem. Phys. 183 (1994) 235–247.
[41] P. Jurkiewicz, J. Sykora, A. Olzynska, J. Humplickova, M. Hof, Solvent relaxation in phospholipid bilayers: principles and recent applications, J. Fluoresc. 15 (2005) 883–894.
[42] P. Jurkiewicz, L. Cwiklik, P. Jungwirth, M. Hof, Lipid hydration and mobility: an interplay between fluorescence solvent relaxation experiments and molecular dynamics simulations, Biochimie 94 (2012) 26–32.
[43] K. Kinosita, A. Ikegami, S. Kawato, On the wobbling-in-cone analysis of fluorescence anisotropy decay, Biophys. J. 37 (1982) 461–464.
[44] S. Kawato, K. Kinosita, A. Ikegami, Dynamic structure of lipid bilayers studied by nanosecond fluorescence techniques, Biochemistry 16 (1977) 2319–2324.
[45] F. Jähnig, Structural order of lipids and proteins in membranes—evaluation of fluorescence anisotropy data, Proc. Natl. Acad. Sci. U. S. A. 76 (1979) 6361–6365.
[46] M.P. Heyn, Determination of lipid order parameters and rotational correlation times from fluorescence depolarization experiments, FEBS Lett. 108 (1979) 359–364.
[47] G. Lipari, A. Szabo, Effect of librational motion of fluorescence depolarization and nuclear magnetic-resonance relaxation in macromolecules and membranes, Biophys. J. 30 (1980) 489–506.
[48] W.L. Jorgensen, J. Tiradorives, The OPLS potential functions for proteins—energy minimizations for crystals of cyclic-peptides and crambin, J. Am. Chem. Soc. 110 (1988) 1657–1666.
[49] J. Chandrasekhar, M. Saunders, W.L. Jorgensen, Efficient exploration of conformational space using the stochastic search method: application to beta-peptide oligomers, J. Comput. Chem. 22 (2001) 1646–1654.
[50] A. Maciejewski, M. Pasenkiewicz-Gierula, O. Cramariuc, I. Vattulainen, T. Rog, Refined OPLS all-atom force field for saturated phosphatidylcholine bilayers at full hydration, J. Phys. Chem. B 118 (2014) 4571–4581.
[51] W.L. Jorgensen, J. Chandrasekhar, J.D. Madura, R.W. Impey, M.L. Klein, Comparison of simple potential functions for simulating liquid water, J. Chem. Phys. 79 (1983) 926–935.
[52] S. Nose, A molecular-dynamics method for simulations in the canonical ensemble, Mol. Phys. 52 (1984) 255–268.
[53] W.G. Hoover, Canonical dynamics—equilibrium phase-space distribution, Phys. Rev. A 31 (1985) 1695–1697.
[54] M. Parrinello, A. Rahman, Polymorphic transitions in single-crystals—a new molecular-dynamics method, J. Appl. Phys. 52 (1981) 7182–7190.
[55] S. Nose, M.L. Klein, Constant pressure molecular-dynamics for molecular-systems, Mol. Phys. 50 (1983) 1055–1076.

[56] U. Essmann, L. Perera, M.L. Berkowitz, T. Darden, H. Lee, L.G. Pedersen, A smooth particle mesh Ewald method, J. Chem. Phys. 103 (1995) 8577–8593.
[57] B. Hess, H. Bekker, H.J.C. Berendsen, J. Fraaije, LINCS: a linear constraint solver for molecular simulations, J. Comput. Chem. 18 (1997) 1463–1472.
[58] S. Miyamoto, P.A. Kollman, SETTLE—an analytical version of the SHAKE and RATTLE algorithm for rigid water models, J. Comput. Chem. 13 (1992) 952–962.
[59] E. Lindahl, B. Hess, D. van der Spoel, GROMACS 3.0: a package for molecular simulation and trajectory analysis, J. Mol. Model. 7 (2001) 306–317.
[60] F. Wennmohs, M. Schindler, Development of a multipoint model for sulfur in proteins: a new parametrization scheme to reproduce high-level ab initio interaction energies, J. Comput. Chem. 26 (2005) 283–293.
[61] E. Falck, M. Patra, M. Karttunen, M.T. Hyvonen, I. Vattulainen, Lessons of slicing membranes: interplay of packing, free area, and lateral diffusion in phospholipid/cholesterol bilayers, Biophys. J. 87 (2004) 1076–1091.
[62] M. Pasenkiewicz-Gierula, T. Rog, K. Kitamura, A. Kusumi, Cholesterol effects on the phosphatidylcholine bilayer polar region: a molecular simulation study, Biophys. J. 78 (2000) 1376–1389.
[63] J.F. Nagle, S. Tristram-Nagle, Structure of lipid bilayers, Biochim. Biophys. Acta Rev. Biomembr. 1469 (2000) 159–195.
[64] N. Kucerka, S. Tristram-Nagle, J.F. Nagle, Structure of fully hydrated fluid phase lipid bilayers with monounsaturated chains, J. Membr. Biol. 208 (2005) 193–202.
[65] R.D. Kaiser, E. London, Location of diphenylhexatriene (DPH) and its derivatives within membranes: comparison of different fluorescence quenching analyses of membrane depth, Biochemistry 37 (1998) 8180–8190.
[66] M. Franova, J. Repakova, P. Capkova, J.M. Holopainen, I. Vattulainen, Effects of DPH on DPPC–cholesterol membranes with varying concentrations of cholesterol: from local perturbations to limitations in fluorescence anisotropy experiments, J. Phys. Chem. B 114 (2010) 2704–2711.
[67] J. Repakova, J.M. Holopainen, M.R. Morrow, M.C. McDonald, P. Capkova, I. Vattulainen, Influence of DPH on the structure and dynamics of a DPPC bilayer, Biophys. J. 88 (2005) 3398–3410.
[68] B.R. Lentz, Use of fluorescent probes to monitor molecular order and motions within liposome bilayers, Chem. Phys. Lipids 64 (1993) 99–116.
[69] J. Aittoniemi, T. Rog, P. Niemela, M. Pasenkiewicz-Gierula, M. Karttunen, I. Vattulainen, Tilt: major factor in sterols' ordering capability in membranes, J. Phys. Chem. B 110 (2006) 25562–25564.
[70] R.F.M. de Almeida, A. Fedorov, M. Prieto, Sphingomyelin/phosphatidylcholine/cholesterol phase diagram: boundaries and composition of lipid rafts, Biophys. J. 85 (2003) 2406–2416.
[71] M.O. Jensen, O.G. Mouritsen, Lipids do influence protein function—the hydrophobic matching hypothesis revisited, Biochim. Biophys. Acta Biomembr. 1666 (2004) 205–226.
[72] N. D'Avanzo, K. Hyrc, D. Enkvetchakul, D.F. Covey, C.G. Nichols, Enantioselective protein–sterol interactions mediate regulation of both prokaryotic and eukaryotic inward rectifier K + channels by cholesterol, Plos One 6 (2011).
[73] Y.D. Paila, S. Tiwari, A. Chattopadhyay, Are specific nonannular cholesterol binding sites present in G-protein coupled receptors? Biochim. Biophys. Acta Biomembr. 1788 (2009) 295–302.